Molecular Dynamics Simulations of Class C β-Lactamase from *Citrobacter freundii*: Insights into the Base Catalyst for Acylation†

Natalia Díaz,* Dimas Suárez, and Tomás L. Sordo

Departamento de Química Física y Analítica, Universidad de Oviedo, C/Julián Clavería, 8, 33006 Oviedo, Asturias, Spain

Received August 11, 2005; Revised Manuscript Received November 11, 2005

ABSTRACT: Herein, we present results from molecular dynamics (MD) simulations of the class C β-lactamase from *Citrobacter freundii* and its Michaelis complex with aztreonam. Four different configurations of the active site were modeled in aqueous solution, and their relative stability was estimated by means of quantum mechanical energy calculations. For the free enzyme, the energetically most stable configurations present a neutral Lys_{67} residue or an anionic Tyr_{150} side chain. Our calculations predict that these two configurations are quite close in terms of free energy, the anionic Tyr_{150} state being favored by ∼1 kcal/mol. In contrast, for the noncovalent complex formed between the *C. freundii* enzyme and aztreonam, the energetic analyses predict that the configuration with the neutral Lys_{67} residue is much more stable than the anionic Tyr_{150} one (∼20 kcal/mol). Moreover, the MD simulations reveal that the neutral Lys_{67} state results in a proper enzyme−aztreonam orientation for nucleophilic attack and in a very stable contact between the nucleophilic hydroxyl group of Ser_{64} and the neutral amino side chain of Lys_{67}. Thus, both the computed free energies and the structural analyses support the assignation of Lys_{67} as the base catalyst for the acylation step in the native form of the *C. freundii* enzyme.

Production of hydrolytic enzymes known as β-lactamases is the most important mechanism through which bacteria have become resistant to β-lactam antibiotics (*1*−*3*). The β-lactamases are traditionally grouped into four classes, A−D, according to their sequence homology (*4*). Classes A, C, and D consist of serine hydrolases whose catalytic action is characterized by a simple acyl−enzyme pathway. In the first step, an acyl−enzyme intermediate is formed between the β-lactam moiety and a conserved serine residue. In the second step, the acyl−enzyme intermediate is hydrolyzed by a water molecule and the active site is regenerated for the next turnover by product loss. The class B β-lactamases are zinc metalloenzymes and catalyze the hydrolysis of nearly all β-lactams, including the versatile broad-spectrum antibacterial carbapenem derivatives.

The serine β-lactamases outnumber the zinc enzymes and are considered a more immediate threat that compromises the future therapeutic usefulness of the β-lactam antibacterial agents (*5*). Among the serine enzymes, the class C β-lactamases are broadly disseminated. They are encoded in the chromosomes of most Gram-negative rods, and recently, they have also been more frequently encountered as plasmid-mediated enzymes. Moreover, many extended-spectrum class C enzymes, which have emerged during the past decade, are able to efficiently hydrolyze the third-generation cephalosporins commonly used to treat serious infections (*6*).

Because of their increasing clinical significance, class C β-lactamases have been intensively studied by means of high-resolution X-ray crystallography, enzyme kinetics, site-directed mutagenesis experiments, and molecular simulations. Crystal structures are available for three class C native enzymes and some of their mutants, alone and in complexes with different ligands (*7*−*22*). These structures show that the class C enzymes share with the other serine β-lactamases a common fold characterized by a two-domain structure formed by a mainly helical domain and an α/β-domain. The active site is found at the interface of the two domains and displays, in all the serine enzymes, a high degree of similarity in the relative position of three conserved motifs. In the class C β-lactamases, these invariant elements correspond to the Ser_{64}-X-X-Lys_{67} sequence, which is located at the amino terminus of a long helix and contains the nucleophilic serine; to the Tyr_{150}-X-Asn_{152} sequence, which is found in a short loop; and to the Lys_{315}-Thr_{316}-Gly_{317} sequence that is situated in strand β7 of a nine-stranded β-sheet.

Site-directed mutagenesis and kinetic experiments resulted in the identification of the residues directly involved in catalysis. Thus, mutations at the conserved Lys_{67} and Tyr_{150} residues have been found to significantly reduce the activity of the enzyme (*23*−*26*), and accordingly, two main reaction mechanisms have been proposed. In these proposals, either a neutral Lys_{67} or an anionic Tyr_{150} activates the nucleophilic Ser_{64} during acylation. In addition, residues Ans_{152}, Lys_{315}, Thr_{316}, and Gly_{317} have been deemed essential according to mutagenesis experiments (*25*, *27*, *28*). In fact, the X-ray structures show that all these active site residues are involved in a dense hydrogen bonding network that is commonly thought to be crucial for catalysis (*26*).

Previous experimental and theoretical results have not been conclusive with regard to the identity of the base catalyst and/or the protonation configuration of the native form of

† This research was supported by the FICyT (Asturias, Spain) via Grant PB02-045 and the Ramon y Cajal program of the MEC (Spain).

* To whom correspondence should be addressed. Phone: +34-985105010. Fax: +34-985103125. E-mail: diazfnatalia@uniovi.es.

10.1021/bi051600j CCC: $33.50
Published on Web 12/17/2005

Chart 1

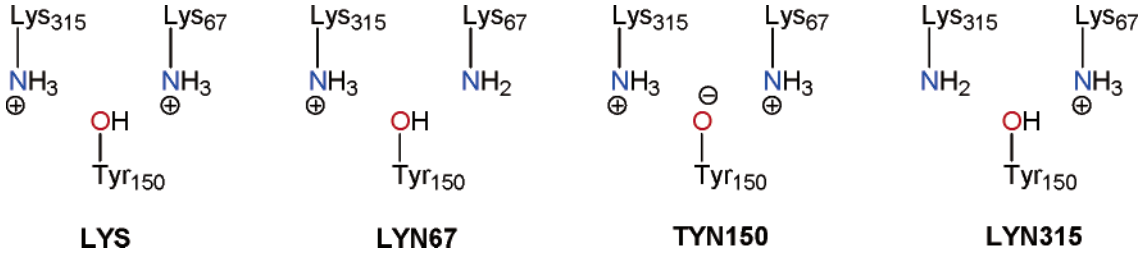

the class C enzymes. For example, the proposed role of an anionic Tyr_{150} as the base catalyst during acylation and hydrolysis seems incompatible with ^{13}C NMR experimental data reported for the class C β-lactamase from *Citrobacter freundii* (*29*). The ^{13}C NMR titration experiments showed that the chemical shift of the Tyr_{150} resonance is almost invariant in the pH range 6−12, suggesting that Tyr_{150} would be protonated during the entire titration of the substrate-free enzyme (the pK_a value could be well above 11). However, this interpretation of the ^{13}C NMR spectra challenges earlier electrostatic Poisson−Boltzmann calculations that predicted an unusually low pK_a value for the Tyr_{150} phenol group in the apoenzyme (4.0−8.3 depending on the protein dielectric constant) (*30*). The same electrostatic calculations provided a pK_a value around 10−11 for Lys_{67}, which seems incompatible with its mechanistic role as the base catalyst. As a result, alternative mechanisms have been proposed in which either the β-lactam carboxylate or the leaving amino group would activate the nucleophile (*15*, *31*, *32*). On the other hand, mixed ab initio quantum mechanical/molecular mechanical (QM/MM)[1] calculations performed on the class C P99 acyl−enzyme intermediate formed with cephalothin have indicated that the state with an anionic Tyr_{150} residue could be slightly more stable than the state with a neutral Lys_{67} (*33*). Nevertheless, the authors notice that the computed energy difference between the two configurations (1.8 kcal/mol) is within the margin of error of the employed methodology.

The interaction between class C β-lactamases and different substrates and inhibitors has been analyzed by X-ray crystallography and molecular dynamics (MD) simulations. Most of the crystal structures obtained for the class C enzymes correspond to acyl−enzyme intermediates with β-lactam inhibitors and poor substrates (*7*, *11*, *14*, *15*). These structures reveal key interactions that contribute to the binding of the degraded β-lactam in the acyl−enzyme intermediate. In addition, the structure of the Ser64Gly mutant of the AmpC enzyme in complex with the β-lactam cephalothin, in its substrate and product forms, has also been determined (*15*). Interestingly, the β-lactam carboxylate group appears to accept a hydrogen bond from the Tyr_{150} side chain in the X-ray structure of the prereactive complex, which in turn precludes the presence of an anionic Tyr_{150} prior to acylation. A similar contact has also been observed in an MD study of the *Enterobacter cloacae* P99 β-lactamase complexed with penicillin G and cephalothin (*34*). In this MD simulation, the hydroxyl group of Ser_{64} was modeled in its anionic form whereas Tyr_{150} was neutral. On the other hand, the conformational flexibility of the acyl−enzyme intermediate formed between the *C. freundii* β-lactamase and the antibiotic aztreonam has been explored by means of MD simulations, showing that the ester carbonyl group of the degraded antibiotic moves in and out of the "oxyanion hole" (*35*), in contrast with the rigidity of the X-ray structure of the acyl−enzyme intermediate that displays the ester carbonyl group well anchored within the oxyanion hole. The flexibility exhibited by the carbonyl group along the MD simulation is in agreement with the multiple conformations assigned to the ester carbonyl group in the corresponding infrared spectra and, according to the authors, suggests that X-ray crystallographic structures may present an incomplete picture of the conformational distribution of bound ligands in the solution phase (*35*).

Clearly, to improve our understanding of the reaction mechanism of the class C β-lactamases, it is necessary to find out which are the actual protonation configurations of the active site residues relevant to catalysis, as well as to identify the most important substrate and inhibitor binding determinants at the pre-reactive Michaelis complex. To fulfill these goals, we decided to perform first an analysis of the protonation configurations of the unbound form of the *C. freundii* class C β-lactamase that could be important according to X-ray analyses, theoretical pK_a calculations, mutagenesis, and kinetic results. Namely, we selected four configurations of the fully solvated enzyme differing in the protonation state of the Lys_{67}, Tyr_{150}, and Lys_{315} residues (see Chart 1) and examined them by means of extended MD simulations and quantum mechanical (QM) calculations. During the simulations, we characterized the interactions between the important functional groups, and the structural and dynamical changes related to protonation and/or deprotonation of the active site residues. The free energy of each configuration was estimated by using semiempirical quantum chemical methodologies to compute enthalpies and solvation energies for protein subsystems, while molecular mechanics calculations were used to account for dispersive interactions and entropic effects.

Subsequently, the complexed form of the *C. freundii* enzyme with aztreonam (AZT) was simulated for the same four configurations of the apoenzyme. Aztreonam, which was the first fully synthetic monocyclic β-lactam antibiotic (*36*), is active against Gram-negative organisms. Moreover, it is highly resistant to hydrolytic turnover by most β-lactamases because the deacylation of the acyl−enzyme intermediate is slow, which has allowed crystallization of the corresponding intermediate formed with the *C. freundii* enzyme (*7*). The analysis of the configurations of the β-lactamase−AZT noncovalent complex resulted in the characterization of the

[1] Abbreviations: AZT, aztreonam; D&C, divide and conquer; DFT, density functional theory; MD, molecular dynamics; QM, quantum mechanical; QM/MM, hybrid quantum mechanical and molecular mechanical; PB, Poisson−Boltzmann; PES, potential energy surface; PDB, Protein Data Bank.

structural and dynamical changes upon inhibitor binding as well as the specific role of key residues in anchoring the ligand. The free energies for the β-lactamase−AZT complexes were also estimated. To better compare with experimental results, a fifth β-lactamase−AZT complex was simulated in which the Lys_{67} residue was mutated into an Arg while the Tyr_{150} side chain was kept unprotonated. Finally, we discuss the ability of our results to help identify the most likely protonation configurations of the native state of the class C enzyme and which residue is best suited for acting as the base catalyst during the acylation process.

METHODS

MD Simulations of the Unbound Form of the C. freundii Class C β-Lactamase. Initial coordinates for the protein atoms and the crystallographic water molecules were taken from the solid-state structure of the *C. freundii* class C enzyme at 2.0 Å resolution (PDB entry 1FR1, chain B) (*7*). The ionizable residues were set to their normal ionization states at pH 7, except Lys_{67}, Tyr_{150}, and Lys_{315} that were ionized according to Chart 1 in the four trajectories examined for the apoenzyme. Histidine residues were protonated at Nδ, with the exception of His_{108} that was protonated at Nϵ in agreement with the contacts observed in the initial X-ray structure. The protein atoms, as well as all the water molecules of the crystal structure, were surrounded by a periodic box of TIP3P (*37*) water molecules that extended 10 Å from the protein. Cl^- counterions were placed by LEaP (*38*) to neutralize the system. This resulted in a total of ∼5602 protein atoms being solvated by 226 X-ray water molecules and 12 577 additional water molecules.

The parm94 version of the all-atom AMBER force field was used to model the system (*39*). To derive the AMBER parameters for the anionic Tyr_{150} residue present in the TYN150 model, a NME-TYR^--ACE peptide was constructed with LEaP. After geometry optimization at the HF/6-31G* level, the corresponding RESP charges of the anionic Tyr residue were obtained by employing a standard two-stage fitting procedure that preserved the parm94 charges of the backbone atoms. Solvent molecules and counterions were initially relaxed by means of energy minimizations and 50 ps of MD. Then the full system was minimized to remove bad contacts in the initial geometry. All the MD simulations were carried out using PMEMD included in the AMBER 8.0 suite of programs (*40*). The time step was chosen to be 1.5 fs, and the SHAKE algorithm was used to constrain all bonds involving hydrogen atoms. A nonbonded cutoff of 10.0 Å was used, and the nonbonded pair list was updated every 25 time steps. The pressure (1 atm) and the temperature (300 K) of the system were controlled during the MD simulation by Berendsen's method (*41*). Periodic boundary conditions were applied to simulate a continuous system. To include the contributions of long-range interactions, the Particle-Mesh-Ewald (PME) method (*42*) was used with a grid spacing of ∼1 Å combined with a fourth-order B-spline interpolation to compute the potential and forces in between grid points.

For all the configurations that were examined, 2.2 ns trajectories were computed and coordinates were saved every 250 time steps. Only the last 1.0 ns of each simulation was analyzed using the CARNAL module of AMBER and some other specific trajectory analysis software developed locally. Structural figures were produced with Molscript (*43*) and Raster3D (*44*).

Chart 2

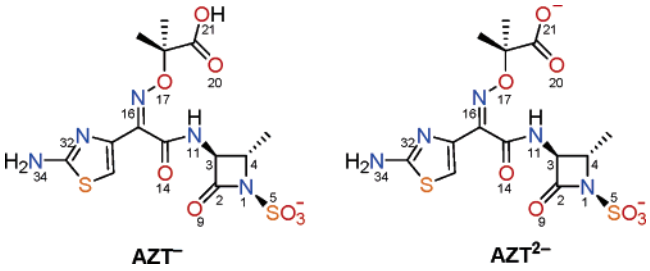

MD Simulations of the Michaelis Complex Formed with Aztreonam. As originally suggested by Oefner et al. in their crystallographic study of the *C. freundii* acyl−enzyme intermediate (*7*), aztreonam was initially modeled as a monoanion with a neutral acylamino side chain and a negatively charged sulfonyl group attached to the β-lactam nitrogen atom (AZT^- in Chart 2). This protonation state is supported by the presence of a direct contact (2.9 Å) observed in the crystal structure between the carboxylic group of the AZT molecule in chain A and the Asp_{123} carboxylate group in chain B. The apparent pK_a values of aztreonam were indirectly determined by solubility measurements, the reported pK_a values for the sulfonyl, amine, and carboxyl groups being −0.7, 2.75, and 3.91, respectively (*45*). In addition, it has been pointed out that aztreonam can exist as a neutral zwitterion, monoanion, and dianion in the pH range from 0 to 8. According to these data, aztreonam would exist as a dianion in aqueous solution at physiological pH. Hence, we also considered a dianionic state for AZT in which both the β-lactam sulfonyl and the carboxylate side chain at C19 were negatively charged (AZT^{2-} in Chart 2).

Initial coordinates for aztreonam were taken from its crystallographic structure (*46*). For the two AZT protonation states, the geometry of the antibiotic was relaxed in aqueous solution at the HF/6-31G* level of theory using the Onsager solvent continuum model as implemented in the Gaussian 98 suite of programs (*47*). Subsequently, atomic charges were computed using the RESP fitting procedure and the gas-phase HF/6-31G* electrostatic potential. Most of the bond, angle, and dihedral parameters of AZT were available from the AMBER force field. However, some structural data required to represent the equilibrium geometry of the β-lactam ring and of the acylamino side chain were extracted from the HF/6-31G*-optimized structure. The van der Waals parameters were taken from the closest existing AMBER atom types using electronic similarity as a guide. In addition, some specific torsion parameters were included to properly reproduce the *syn* conformation of the *N*-SO_3^- group with respect to the acylamino side chain. These torsion parameters were adjusted against ab initio conformational energies and geometries obtained for a small model compound (3-formylamino-4-methyl-2-azetidine-1-sulfonate ion) at the MP2/6-31+G** level. The aztreonam parameters in a format suitable for the LEaP program are given in the Supporting Information.

The LYS, LYN67, TYN150, and LYN315 configurations of the *C. freundii* enzyme were modeled in the presence of an aztreonam molecule bound to the active site. The initial

structure for the enzyme−inhibitor complex was built using the X-ray crystal structure of the corresponding acyl−enzyme intermediate (PDB entry 1FR6, chain A) (*7*). After having superposed the acyl−enzyme structure onto the crystallographic structure of the native enzyme (PDB entry 1FR1, chain B), we extracted the coordinates of the degraded aztreonam molecule, and the β-lactam ring was rebuilt by molecular modeling. The 1FR1 structure augmented with the coordinates of aztreonam was then employed as the starting point for the class C enzyme−AZT configurations following simulation protocols identical to those used for the unbound models. After mutating the Lys_{67} residue in the 1FR1 structure into an arginine residue using LEaP, we followed the same computational approach to carry out the ARG67−TYN150−AZT simulation.

Energetic Analyses of the MD Trajectories. To calculate the average free energies for the simulated class C configurations, we employed a variant of the so-called MM-PBSA approach (*48*, *49*) in which the enthalpy and solvation energy terms are computed by means of semiempirical QM calculations (QM-PBSA calculations). Most of the QM-PBSA computational details have been previously described (*50*), and therefore, they are briefly summarized herein.

First, a set of 50 representative structures were extracted every 20 ps along the last 1 ns of the simulation time of each MD trajectory, and were subjected to PM3/AMBER energy minimization. For the apoenzyme, the QM region comprised the Ser_{64}, Lys_{67}, Ala_{220}, Thr_{316}, and Ser_{318} residues, and the side chains of Tyr_{150}, Asn_{152}, Glu_{272}, and Lys_{315}. For the AZT-complexed structures, the QM region also included the AZT inhibitor. From the QM/MM relaxed structures, we selected protein subsystems (∼2100 atoms) that were composed of all residues within ∼15 Å of the Oγ@Ser_{64} atom.

Second, the average free energy of the protein subsystems was estimated according to the following equation:

$$\bar{G} \approx \bar{H}_{QM} + \bar{E}_{disp} + \Delta\bar{G}_{solv} - T\bar{S}_{MM} \qquad (1)$$

where $\bar{G}$ is the calculated average free energy, $\bar{H}_{QM}$ is the average QM heat of formation of the solute that accounts for intraprotein and enzyme−ligand effects, $\bar{E}_{disp}$ is an empirical energy that takes into account the attractive dispersive interactions, $\Delta\bar{G}_{solv}$ is the average solvation energy, which is calculated using a QM Hamiltonian coupled with a continuum model, and $-T\bar{S}_{MM}$ is the solute entropy which is estimated by molecular mechanics normal mode calculations.

The semiempirical QM energy terms in eq 1, $\bar{H}_{QM}$ and $\Delta\bar{G}_{solv}$, are computed efficiently on systems containing thousands of atoms by using the divide and conquer (D&C) SCF algorithm (*51*) as implemented in DIVCON (*52*, *53*). We performed single-point PM3 calculations (*54*) on the protein subsystems, while solvent effects were included within the semiempirical QM methodology by merging the D&C algorithm with the PB equation (*55*). We used an interior dielectric constant (protein) of 1 and an exterior value (water) of 80. An $\epsilon_{protein}$ value of 1 is adequate given that (a) electronic polarization effects are taken into account by the semiempirical QM calculations and (b) polarization effects related to field-induced nuclear reorientations in the macromolecule are at least taken into account in the structures collected during the MD sampling (*56*). Further details of the D&C calculations are given elsewhere (*50*).

The dispersion energy contribution, E_{disp}, was computed using an empirical formula that has been introduced by Elstner et al. (*57*) to extend their approximate DFT method (*58*) for the description of dispersive interactions, which are normally neglected in both the DFT and semiempirical QM methods. The E_{disp} expression consists basically of a C_6/R^6 term, which is appropriately damped for short R distances. The corresponding C_6 coefficients for each pair of interacting atoms are calculated from experimental atomic polarizabilities (*59*) so that the total E_{disp} energy can be consistently added to the energy expression of the DFT and semiempirical methods. In this work, we used the same parameters and combination rules described by Elstner et al. (*57*), which in turn are based on previous work by Halgren (*60*). In the Supporting Information (Figure S1), we show that the semiempirical PM3 method complemented with the E_{disp} term is capable of reproducing fairly well the interaction energies between pairs of hydrophobic residues, as evaluated by high-level correlated ab initio calculations (*61*). Inclusion of the E_{disp} term in the QM-PBSA calculations ensures a balanced description of the free energy changes due to the enzyme−ligand union and/or protein conformational changes.

Solute entropic contributions were estimated for the series of protein subsystems with ∼2000 atoms by using the *nmode* module of the AMBER 8.0 package (*40*). This program uses the normal modes and standard statistical thermodynamical formulas to estimate entropic contributions. Prior to the normal mode calculations, the geometries of the subsystems described by their AMBER representations were minimized until the root-mean-square deviation of the elements in the gradient vector was less than 10^{-5} kcal mol^{-1} Å^{-1}.

To calibrate the performance of the semiempirical QM Hamiltonian (PM3) as applied to our particular problem, we optimized in aqueous solution a series of small cluster models relevant to the modeled class C active site configurations at the B3LYP/6-31G*, B3LYP/6-31+G**, and PM3 levels of theory. From these calculations, we derived "high-level correction" terms to the relative free energies of the protein models, as explained in the Supporting Information.

RESULTS

RMSD Values and RMS Flexibility for the Apoenzyme. In Table S1 of the Supporting Information, the heavy atom root-mean-square deviations (RMSDs) of the *C. freundii* class C β-lactamase simulations relative to its initial crystal structure are given for the most relevant structural elements. Data in this table show that the structural changes in the protein taking place during the course of the MD simulations were moderate (1.5−1.8 Å for all heavy atoms).

The LYS trajectory, which presents an additional positive charge in the active site as compared with the other three simulations, together with the LYN315 trajectory exhibits the largest RMSD values (1.7−1.8 Å). The segregation of the RMSD values into distinct structural elements shows that the largest deviations among the protein configurations arise in the β7 strand, the β6−β7 turn, and the C-terminal α-helix. For the LYS simulation, these changes can be traced to the backbone flexibility of the residues situated at the "oxyanion hole" (Gly_{317}-Ser_{318}), which are adjacent to the important

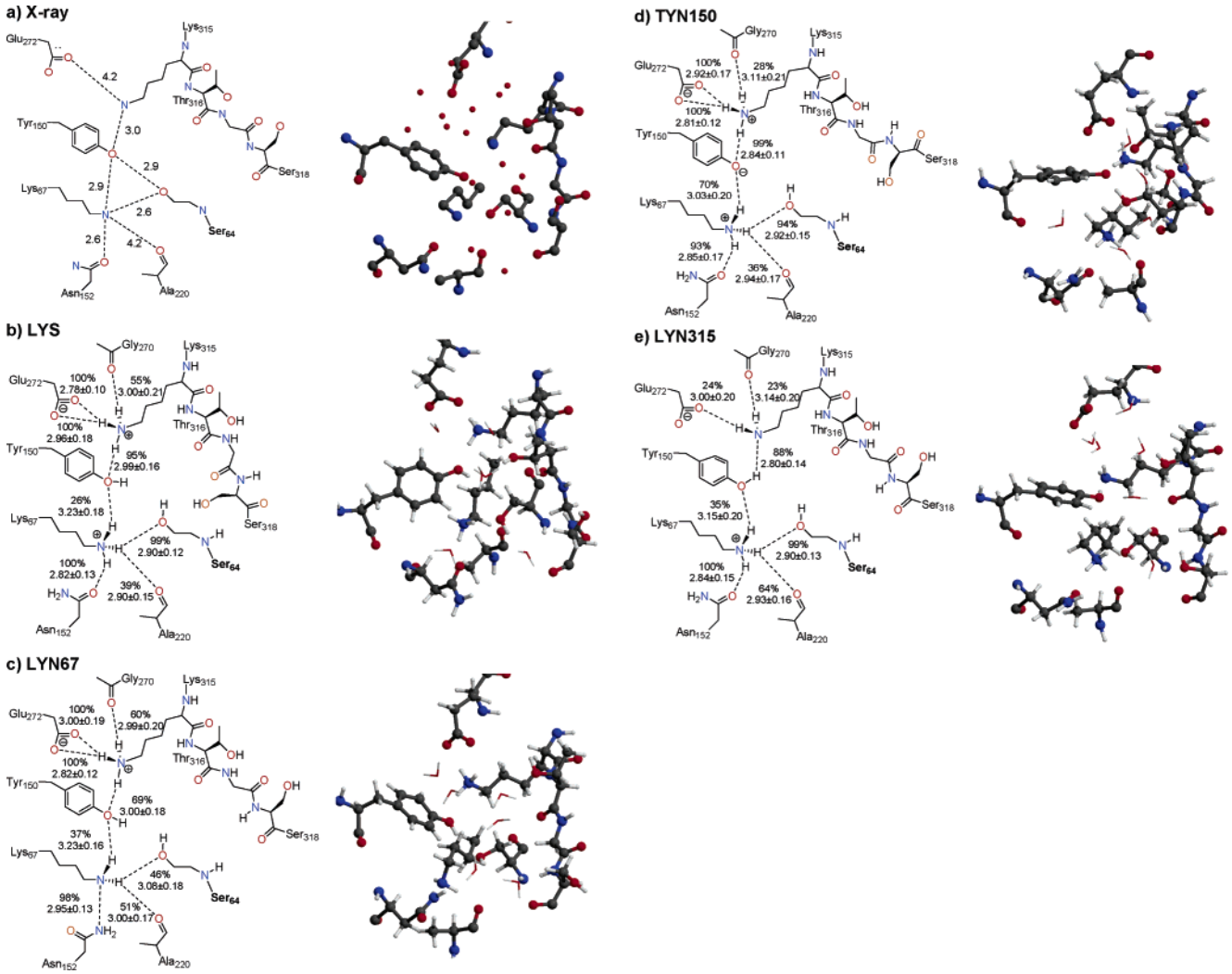

FIGURE 1: Schematic representation of the main interresidue contacts observed in the *C. freundii* class C β-lactamase active site: (a) in the 1FR1 X-ray structure and (b−e) along the four trajectories computed for the apoenzyme. A snapshot of the active site extracted from each simulation has been produced with Molscript and Raster3D.

residues in the active site, and to the side chain flexibility of Arg_{349}, which is located in the terminal α-helix and contacts with the β6 strand (see below). On the other hand, the root-mean-square flexibility (RMSF), calculated by comparing the instantaneous protein structure to the average one, is similar for the different trajectories (∼0.8−0.9 Å). Finally, the active site residues show RMSD and RMSF values that do not change dramatically across the four trajectories (0.8−1.0 and 0.4−0.6 Å, respectively).

Structure of the Active Site. In the X-ray structure, the class C active site is characterized by a dense hydrogen bonding network that interconnects the catalytically relevant residues (Ser_{64}, Lys_{67}, Tyr_{150}, Asn_{152}, Lys_{315}, Ser_{318}, etc.) and some solvent molecules (see Figure 1). Thus, the hydroxyl group of the nucleophilic serine (Ser_{64}) interacts with the side chains of Lys_{67} (Ser_{64} Oγ···Nζ Lys_{67} = 2.6 Å) and Tyr_{150} (Ser_{64} Oγ···Oη Tyr_{150} = 2.9 Å) and with a water molecule (Ser_{64} Oγ···O Wat = 2.4 Å) that is partially located in the oxyanion hole formed by the backbone NH groups of Ser_{64} and Ser_{318}. The lysine residue of the first conserved motif (Lys_{67}) also interacts with the Asn_{152} side chain (Lys_{67} Nζ···Nδ Asn_{152} = 2.6 Å), while Tyr_{150} is H-bonded to both Lys_{67} and Lys_{315} with Oη···Nζ distances of 2.9−3.0 Å. Lys_{315} also makes a contact with the backbone carbonyl group of Thr_{316} (Lys_{315} Nζ···O Thr_{316} = 2.9 Å) and, through a water molecule, with the carboxylate group of the invariant Glu_{272}.

Figure 1 shows representative snapshots extracted from the four MD simulations as well as schematic representations of the most stable H-bond contacts, including their percentages of occurrence and their average distances. In Table S2 of the Supporting Information, we collect the average values for the most significant active site interatomic distances.

With regard to the nucleophilic serine residue, a stable Ser_{64} Oγ···HNζ Lys_{67} H-bond contact is present in the LYS, TYN150, and LYN315 trajectories (94−99% of occupancy and 2.9 Å average distance), but it has an abundance of only 46% along the LYN67 trajectory (see Figure 1). The interaction between the Ser_{64} and Tyr_{150} side chains, observed in the crystallographic structure, was poorly stable along the four simulations (7−34% of abundance). On the other hand, the Ser_{64} hydroxyl group is hydrated by two to four water molecules in all the trajectories. Some of these water molecules are roughly located within the oxyanion hole connecting the Ser_{64} side chain with the Ser_{64} and Ser_{318} backbone amino groups.

The Lys_{67} and Asn_{152} residues give stable contacts in all the simulations. For example, a Lys_{67} NζH···Oδ Asn_{152} H-bond contact, which is clearly present in the initial X-ray

structure, is stable along the LYS, TYN150, and LYN315 trajectories (2.8 Å, 93−100% of occupancy). For the LYN67 model, however, the Asn_{152} side chain internally rotates after 1.2 ns to give an unexpected Lys_{67} N$\zeta\cdots$HNδ Asn_{152} interaction that remained perfectly stable during the rest of the simulation time (98% of occupancy and 2.9 Å). On the other hand, the $Lys_{67}\cdots Tyr_{150}\cdots Lys_{315}$ association, observed in the initial X-ray structure, is stable only along the TYN150 trajectory through ionic contacts (Lys N$\zeta H_3^+\cdots{}^-$Oη Tyr_{150}) between the phenolic group of Tyr_{150} and the positively charged ammonium groups of Lys_{67} and Lys_{315}. The $Lys_{67}\cdots Tyr_{150}\cdots Lys_{315}$ association is marginally stable along the other three trajectories, although Tyr_{150} remains H-bonded to the Lys_{315} side chain (69−95% of occupancy; see Figure 1).

According to the computed radial distribution function of solvent molecules, the Oη@Tyr_{150} atom also interacts with one water molecule. In addition, the orientation of the Tyr_{150} side chain is controlled by hydrophobic interactions with the adjacent Tyr_{112} side chain. The average distance between the center of mass of the corresponding aromatic rings (4.8 Å) and the angle between their planes (50−54°) are indicative of correlated motions during the four trajectories.

The second lysine residue in the active site, Lys_{315}, also interacts with the carboxylate group of the conserved Glu_{272} residue in the LYS, LYN67, and TYN150 simulations (100% of occupancy), although a direct $Lys_{315}\cdots Glu_{272}$ salt bridge is not observed in the X-ray structure. When the Lys_{315} residue is modeled in its neutral state (LYN315), the $Lys_{315}\cdots Glu_{272}$ contact is less stable (24% of occupancy) and the Lys_{315} side chain becomes more solvent exposed: three water molecules are located within the first solvation shell around the Nζ@Lys_{315} atom during the LYN315 simulation, whereas one or two waters were observed for the other three trajectories.

Interestingly, the protonation state of the active site residues influences the mobility and average conformation of the structural motifs close to the active site region. For example, the oxyanion hole is partially distorted in the LYS and TYN150 trajectories as a result of a rotation (∼100°) about the Cα@Gly_{317}−C@Gly_{317} bond in the β7 strand occurring at the beginning of the two simulations. Moreover, an additional rotation about the Cα@Gly_{320}−C@Gly_{320} bond modifies the conformation of the β6−β7 turn in the LYS trajectory. Along this same trajectory, an anchorage point between the C-terminal α-helix and the β6 strand, constituted by a hydrogen bond interaction between the Arg_{349} guanidinium and the Ser_{324} carbonyl groups, is lost and the Arg_{349} side chain moves away from the catalytic center to become more solvent accessible. These and other changes might be triggered by long-range electrostatic forces that can particularly affect the relatively buried Arg_{349} side chain.

Energetic Analyses of the MD Trajectories. Prior to the energetic analyses, the structure of the active site in selected snapshots along the MD trajectories was relaxed via PM3/AMBER energy minimizations. In general, the QM/MM structures, in which the Ser_{64}, Lys_{67}, Tyr_{150}, Asn_{152}, Ala_{220}, Glu_{272}, Lys_{315}, Thr_{316}, and Ser_{318} residues were described by the PM3 method, were structurally similar to those generated along the MD simulations using the MM force field representation. Subsequently, we performed single-point PM3 D&C−PB calculations, empirical calculations of the dispersive interactions, and MM normal mode calculations on subsystems comprising approximately one-third of the protein. These energetic terms, whose average values are shown in Table 1, were combined to estimate the QM-PBSA free energy of the various protein configurations.

Table 1: PM3-Based Free Energy Components[a] of the Class C β-Lactamase[b]

system	E_{disp}	H	ΔG_{solv}	G_{total}[c]
LYS	−1240.1 (1.2)	−5321.1 (7.4)	−1212.5 (4.5)	−9457.3 (6.9)
LYN67	−1257.6 (1.4)	−5489.3 (6.5)	−1147.2 (3.3)	−9576.2 (6.8)
	0	*0*	*0*	*0*
LYN315	−1244.0 (1.1)	−5443.9 (7.1)	−1189.5 (3.0)	−9559.8 (6.6)
	14	*45*	*−42*	*16*
TYN150	−1256.1 (1.3)	−5476.3 (7.3)	−1157.0 (5.1)	−9572.9 (6.3)
	2	*13*	*−10*	*3*

[a] In kilocalories per mole. [b] The standard error of the mean values is given in parentheses. Relative differences in the mean values with respect to the LYN67 ones are in italics. [c] Including the entropy corrections from MM normal mode calculations on subsystems.

The average QM-PBSA free energy differences between the TYN150 and LYN315 configurations with respect to the LYN67 one are 3 and 16 kcal/mol (−1 and 17 kcal/mol, respectively, after adding the corresponding "high-level correction" term; see the Supporting Information), respectively. From these ΔG values, it seems that the anionic state of the Tyr_{150} residue would be energetically favored in the native form of the class C β-lactamase. It must be noted, however, that the small ΔG between LYN67 and TYN150 is lower, in absolute value, than the fluctuations of the individual free energies (∼6−7 kcal/mol), which are expressed in terms of the standard error of the mean values (see Table 1). Therefore, both states could be energetically accessible. On the other hand, the magnitude of the ΔG associated with the LYN315 state, 17 kcal/mol, allows us to safely discard this protein configuration as a model of the native form of the *C. freundii* enzyme. We also estimated the relative stability of the LYN67 configuration with respect to the LYS model, in which both Lys_{67} and Lys_{315} are positively charged, by considering the free energy change for the proton dissociation process connecting formally the LYS and LYN67 states, that is, LYS → LYN67 + H^+(aq). If the thermodynamic data for H^+(aq) are combined with the G values for the LYS and LYN67 states in Table 1, the free energy change for this process is largely negative, −20 kcal/mol (−14 kcal/mol if the high-level correction is included). According to these QM-PBSA free energy analyses, the LYS configuration is very unlikely to represent the unbound form of the class C enzyme in solution.

Inspection of the free energy components in Table 1 suggests that the larger stability of the LYN67 and TYN150 configurations with respect to LYN315 and LYS ones is mainly due to stronger intraprotein contacts for which the H and E_{disp} terms account. Part of this energetic preference could be due to the smaller structural deviations of the LYN67 and TYN150 models with respect to the initial X-ray structure.

Structural Analyses of the Class C β-Lactamase−AZT Complexes. The Michaelis complex formed between the *C. freundii* class C β-lactamase and aztreonam was modeled in the four different configurations of the active site studied for the apoenzyme. As mentioned in Methods, aztreonam was simulated both as a monoanion (AZT^-) and as a dianion

(AZT^{2-}) (see Chart 2). Tables S5 and S6 of the Supporting Information list the RMSD and RMSF values for these configurations.

Comparison of the RMSD values in Tables S5 and S6 with those in Table S1 shows that AZT binding does not induce large changes in the global structure of the protein. The average RMSD values of the different class C−AZT configurations are practically identical, in contrast with the ampler structural deviations exhibited by the LYN315 and LYS states in the free form of the enzyme. A similar effect is observed in the RMSF values (0.8−0.9 Å). In fact, location of AZT at the interface of the two domains of the enzyme reduces the active site flexibility in all the configurations. Therefore, these observations suggest that, in the presence of the inhibitor, the class C enzyme is slightly rigidified.

The protonation state of AZT largely influences the orientation of the inhibitor within the *C. freundii* active site. When the antibiotic is modeled in its dianionic form (AZT^{2-}), its negatively charged carboxylate and sulfonyl groups interact with the positively charged Arg_{204} and Arg_{349} guanidinium groups of the enzyme, respectively. As a consequence, the four configurations, LYS−AZT^{2-}, LYN67−AZT^{2-}, TYN150−AZT^{2-}, and LYN315−AZT^{2-}, can be considered nonreactive states because the nucleophilic serine side chain is not properly located with respect to the β-lactam amide group and/or is not interacting with the putative base catalyst (see Figure S3 of the Supporting Information). In contrast, three of the four simulations performed with the monoanionic AZT^{-} present a relative orientation of the Ser_{64} side chain and the β-lactam ring favorable for catalysis (e.g., the AZT C2···Oγ Ser_{64} distances are 3.2−3.3 Å, while the AZT N1−C2−O9···Oγ Ser_{64} dihedral angles are 83−88°). For the sake of brevity, the structural and energetic analyses of the LYS−AZT^{2-}, LYN67−AZT^{2-}, TYN150−AZT^{2-}, and LYN315−AZT^{2-} configurations are summarized in the Supporting Information (Tables S6 and S7 and Figure S3). Next we present in more detail the results obtained for the β-lactamase−AZT^{-} complexes with anionic aztreonam: LYS−AZT^{-}, LYN67−AZT^{-}, TYN150−AZT^{-}, and LYN315−AZT^{-}.

Interresidue Contacts in the β-Lactamase−AZT Complexes. Figure 2 shows schematic representations of the relevant H-bond contacts observed in the β-lactamase active site and characteristic snapshots extracted from the MD trajectories. In general, binding to AZT introduces slight changes in the active site interresidue contacts previously described for the apoenzyme. Thus, the LYN67−AZT^{-} trajectory presents a stable Ser_{64} Oγ**H**···:Nζ Lys_{67} contact (2.72 ± 0.10 Å, 100%) that replaces the Asn_{152} NδH_2···:Nζ Lys_{67} interaction observed in the LYN67 simulation. The Lys_{67} side chain is H-bonded to the carbonyl group of the Asn_{152} side chain in all the trajectories of the complex (87−100% of occupancy), and its contact with the carbonyl group of Ala_{220} is clearly reinforced in the LYS−AZT^{-} and LYN67−AZT^{-} states (see Figure 2). In addition, ligand binding reduces specifically the flexibility of the oxyanion hole. For example, the rotation about the Cα@Gly_{317}−C bond observed in the LYS and TYN150 simulations of the apoenzyme does not take place in the AZT complexes, the oxyanion hole maintaining its initial conformation along the four trajectories.

β-Lactamase−AZT Binding Determinants. Monobactams, like aztreonam, are characterized by a β-lactam cycle that is not fused to additional rings such as in other β-lactam antibiotics. Binding determinants of AZT should be localized in the four-membered β-lactam ring and in the acylamino side chain. Our simulations show that the stability of the enzyme−inhibitor contacts in the Michaelis complexes and the relative orientation between the nucleophilic serine and the β-lactam cycle depend on the configuration of the active site residues. The relative orientation of the reactive groups together with the presence of long-lived contacts between the nucleophilic serine and a potential base catalyst (the β-lactam sulfonyl group or the side chain of Lys_{67}, Tyr_{150}, or Lys_{315}) allows us to assess the prereactive character of each configuration.

Along the LYS−AZT^{-} trajectory, the antibiotic molecule shifts and changes its initial orientation in the β-lactamase active site. Thus, the β-lactam carbonyl moiety is replaced in the oxyanion hole by one of the oxygen atoms of the negatively charged β-lactam sulfonyl group (AZT SO_3^-···HN Ser_{318}, 2.98 ± 0.16 Å and 79% of occupancy). In addition, the AZT SO_3^- group also interacts with the nucleophilic serine (2.87 ± 0.19 Å, 88%) and with the side chains of Ser_{318} (2.76 ± 0.15 Å, 100%) and Asn_{346} (2.89 ± 0.14 Å, 92%). The carbonyl group of the acylamino side chain interacts with the Asn_{152} NδH_2 group by means of a water molecule (78% of the snapshots).

In principle, the aztreonam *N*-SO_3^- group is the only group capable of activating the Ser_{64} hydroxyl group in the LYS configuration. Moreover, as mentioned above, both groups interact through a stable H-bond contact along the LYS−AZT^{-} trajectory. However, the nucleophilic Ser_{64} side chain is not properly positioned to react toward the β-lactam ring amide group because both groups are nearly coplanar (the average AZT N1−C2−O9···Oγ Ser_{64} torsional angle is 30 ± 14°). The average AZT C2···Oγ Ser_{64} distance (4.20 ± 0.30 Å) and AZT C2···Oγ−Cβ Ser_{64} angle (133 ± 7°) further confirm this point. Thus, we conclude that AZT adopts a nonreactive configuration in the β-lactamase active site when both Lys_{67} and Lys_{315} are protonated.

The LYN67−AZT^{-} simulation is characterized by stable Ser_{64} NH···O9 AZT (2.83 ± 0.11 Å, 100%) and Ser_{318} NH···O9 AZT (2.82 ± 0.10 Å, 100%) H-bond contacts, which maintain the β-lactam carbonyl group within the oxyanion hole. The AZT sulfonyl group is in contact with the Ser_{318} and Asn_{346} side chains (occupancies of 100 and 98%, respectively) and, through a one-water bridge, with the Tyr_{150} hydroxyl group [AZT SO_3^-···(H_2O)···HOη Tyr_{150}, 53% occupancy]. On the other hand, the acylamino carbonyl group of AZT interacts with the Asn_{152} side chain (39 and 36% of direct and water-mediated contacts, respectively), while the exocyclic amino group interacts with the hydroxyl group of Ser_{212} (3.07 ± 0.19 Å, 63%).

From a mechanistic point of view, the LYN67 configuration is characterized by the presence of a neutral lysine in the class C active site (Lys_{67}), which could act as a base catalyst by activating the Ser_{64} hydroxyl group. The stability of the Ser_{64} Oγ**H**···:Nζ Lys_{67} H-bond (2.72 ± 0.10Å, 100%) along the LYN67−AZT^{-} trajectory supports this hypothesis. Moreover, the short AZT C2···Oγ Ser_{64} distance (3.10 ± 0.18 Å), the average value of the AZT C2···Oγ−Cβ Ser_{64} angle (105 ± 7°), and the torsional AZT N1−C2−O9···Oγ

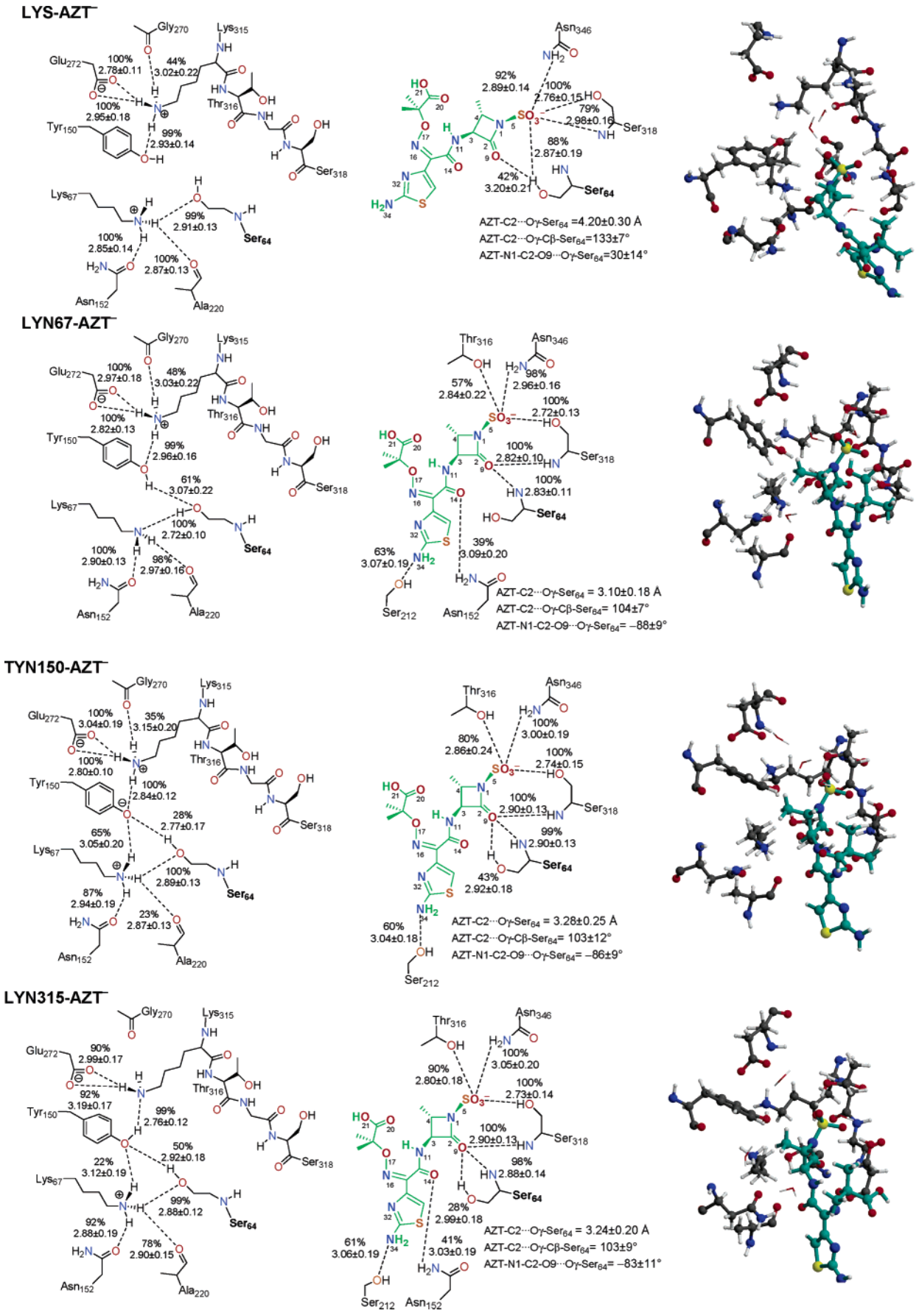

FIGURE 2: Schematic representation of the main interresidue contacts and enzyme−inhibitor binding determinants observed along the four trajectories computed for the Michaelis complex formed between aztreonam (AZT^-) and the *C. freundii* class C β-lactamase enzyme. A snapshot of the active site extracted from each simulation with aztreonam colored green has been produced with Molscript and Raster3D.

Table 2: PM3-Based Free Energy Components[a] of the Class C β-Lactamase Complexed with Aztreonam[b]

system	E_{disp}	H	ΔG_{solv}	G_{total}[c]
LYS−AZT$^-$	−1304.6 (1.0)	−5765.2 (6.5)	−1083.0 (3.0)	−9867.6 (5.7)
LYN67−AZT$^-$	−1301.3 (0.8)	−5868.5 (7.4)	−1081.9 (3.6)	−9967.0 (6.3)
	0	*0*	*0*	*0*
LYN315−AZT$^-$	−1306.8 (1.5)	−5860.7 (7.1)	−1056.7 (4.2)	−9939.7 (5.5)
	−5	*8*	*25*	*27*
TYN150−AZT$^-$	−1290.0 (1.3)	−5858.0 (8.1)	−1077.0 (4.9)	−9942.6 (7.1)
	11	*5*	*5*	*24*

[a] In kilocalories per mole. [b] The standard error of the mean values is given in parentheses. Relative differences in the mean values with respect to the LYN67−AZT$^-$ ones are in italics. [c] Including the entropy corrections from MM normal mode calculations on subsystems.

Ser_{64} angle (−88 ± 9°) confirm that the Ser_{64} side chain is well positioned to attack the amide group of the β-lactam ring.

The TYN150−AZT$^-$ trajectory also shows stable contacts between the β-lactam carbonyl group and the oxyanion hole (Ser_{64} NH···O9 AZT = 2.90 ± 0.13 Å, 99%, and Ser_{318} NH···O9 AZT = 2.90 ± 0.13 Å, 100%). In this case, the AZT sulfonyl group interacts with the Thr_{316} and Ser_{318} hydroxyl groups (2.86 ± 0.24 Å, 80%, and 2.74 ± 0.15 Å, 100%, respectively), with the Asn_{346} side chain (3.00 ± 0.19 Å, 100%), and through water-mediated contact with the anionic Tyr_{150} side (58% of occupancy). Again, the AZT acylamino side chain remains H-bonded to Asn_{152} (48% of water-mediated contacts) and to Ser_{212} (AZT $N34H_2$···Oγ Ser_{212} = 3.04 ± 0.18 Å, 60%).

The average values of the AZT C2···Oγ Ser_{64} distance (3.28 ± 0.25 Å) together with the AZT C2···Oγ−Cβ Ser_{64} and AZT N1−C2−O9···Oγ Ser_{64} angles (103 ± 12° and −86 ± 9°, respectively) show that the Ser_{64} hydroxyl group is well positioned to attack the amide group of the β-lactam ring along the TYN150−AZT$^-$ trajectory. The anionic Tyr_{150} residue seems to be stabilized in the β-lactamase active site by means of ionic contacts with the Lys_{67} and Lys_{315} ammonium groups (see Figure 2). Although Tyr_{150} could act as the base catalyst, we found that the charged Lys_{67} ammonium group competes with the Ser_{64} side chain in interacting with the anionic Tyr_{150}, which shows that only the 28% of the TYN150−AZT$^-$ trajectory presents a direct Ser_{64} OγH···$^-$Oη Tyr_{150} contact.

The fourth simulation of the β-lactamase−AZT Michaelis complex corresponds to the LYN315 configuration. In this case, the β-lactam carbonyl group is again properly positioned within the oxyanion hole. The AZT SO_3^- group establishes stable H-bonds with Thr_{316}, Ser_{318}, and Asn_{346} (90−100% of occupancy), and the AZT acylamino side chain interacts with Asn_{152} (41 and 46% of direct and water-mediated contacts, respectively) and with Ser_{212} (3.06 ± 0.19 Å, 61%). The nucleophilic Ser_{64} group gives alternating H-bond interactions with the Tyr_{150} side chain (2.92 ± 0.18 Å, 50%), with the AZT SO_3^- group (3.10 ± 0.22 Å, 20%), and with the β-lactam carbonyl group (2.99 ± 0.18 Å, 28%).

The LYN315−AZT$^-$ simulation indicates that the neutral Lys_{315} amino group could act as the putative base catalyst through a Ser_{64} OγH···Tyr_{150} OηH···:H_2Nζ Lys_{315} bridged interaction. The Tyr_{150}···Lys_{315} contact was perfectly stable (2.76 ± 0.12 Å, 99%), but the second hydrogen bond (Ser_{64}···Tyr_{150}) existed only during half of the simulation time. Hence, the large flexibility of the contacts displayed by the Ser_{64} hydroxyl group suggests that the LYN315−AZT$^-$ configuration should be less reactive than the LYN67−AZT$^-$ one, although the AZT C2···Oγ Ser_{64} distance (3.24 ± 0.20 Å) and the AZT C2···Oγ−Cβ Ser_{64} and AZT N1−C2−O9···Oγ Ser_{64} angles (103 ± 9° and −83 ± 11°, respectively) seem optimal for nucleophilic attack.

Energetic Analyses of the Class C β-Lactamase−AZT Complexes. The thermodynamic analyses were repeated for the protein subsystems in the different noncovalent complexes following the QM-based computational scheme after having partially relaxed the selected snapshots by means of QM/MM energy minimizations. Examination of the average values of some QM/MM distances between the AZT inhibitor and important residues in the β-lactamase active site showed that the QM/MM relaxation does not alter the identity and properties of the important H-bond interactions that anchor the β-lactam to the active site (data not shown for brevity).

Table 2 shows the average heats of formation, dispersion energies, solvation energies, and free energies of the β-lactamase−AZT complexes. Most interestingly, the presence of the antibiotic stabilizes preferentially the LYN67−AZT$^-$ state that is now 24 and 27 kcal/mol below TYN150−AZT$^-$ and LYN315−AZT$^-$, respectively, in terms of their mean G values. Addition of the high-level correction terms derived from the test calculations to the QM-PBSA G values preserves the energetic preference for the LYN67−AZT$^-$ state, which remains 20 and 28 kcal/mol below TYN150−AZT$^-$ and LYN315−AZT$^-$, respectively. On the basis of these relative free energy differences, it is clear that neither the TYN150−AZT$^-$ nor the LYN315−AZT$^-$ state would represent the ground state of the Michaelis complex between the class C enzyme and AZT.

To determine if the presence of the AZT inhibitor can change the global charge distribution of the class C β-lactamase active site by stabilizing energetically the LYS−AZT$^-$ complex with respect to the LYN67−AZT$^-$ complex, we considered the formal proton dissociation process LYS−AZT$^-$ → LYN67−AZT$^-$ + H$^+$(aq), which has a ΔG value of −1.5 kcal/mol as estimated semiempirically. The "corrected" value would be 4.7 kcal/mol. Comparison with the corresponding ΔG value for the acid dissociation process in the absence of the inhibitor (−14.2 kcal/mol) points out that the negatively charged AZT molecule tends to favor the LYS state. However, this effect would not be enough for the LYS−AZT$^-$ state to become the most populated one at physiological pH (the corrected ΔG value for the LYS−AZT$^-$ → LYN67−AZT$^-$ + H$^+$ process corresponds to an intrinsic pK_a for Lys_{67} of only 4.5). Moreover, the enzyme−inhibitor binding determinants in the LYS−AZT$^-$ model are not favorable for catalysis (see above). Therefore, we propose that the LYN67−AZT$^-$ model will be the kinetically active configuration of the β-lactamase−AZT complex.

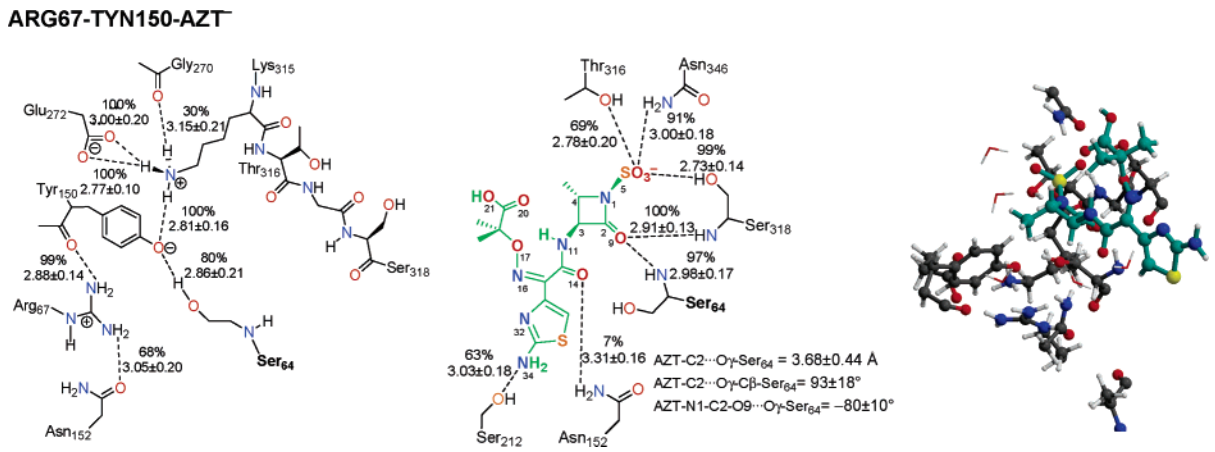

FIGURE 3: Schematic representation of the main interresidue contacts and enzyme−inhibitor binding determinants observed along the ARG67−TYN150−AZT⁻ trajectory. A snapshot of the active site extracted from each simulation with aztreonam colored green has been produced with Molscript and Raster3D.

Simulation of the Lys67Arg Mutant in the ARG67−TYN150−AZT⁻ Configuration. The Lys67Arg mutant of the *C. freundii* class C β-lactamase complexed with aztreonam (AZT⁻) was simulated in the ARG67−TYN150 configuration, which presents an anionic Tyr_{150} located in the active site. The MD simulation shows that the Lys67Arg mutation does not drastically modify the structure of the enzyme. Thus, the RMSD and RMSF values obtained from the ARG67−TYN150−AZT⁻ simulation are very similar to those computed for the TYN150−AZT⁻ state (see Table S5 of the Supporting Information).

Figure 3 presents a schematic representation of the relevant H-bond contacts observed at the β-lactamase active site as well as a characteristic snapshot extracted from the ARG67−TYN150−AZT⁻ trajectory. In this simulation, the Arg_{67} side chain is accommodated well in the active site, establishing stable H-bond interactions with the Asn_{152} side chain (3.05 ± 0.20 Å, 68%) and with the backbone carbonyl group of Tyr_{150} (2.88 ± 0.14 Å, 99%). The nucleophilic Ser_{64} side chain mainly interacts with the anionic Tyr_{150} side chain (2.86 ± 0.21 Å, 80%) and is well oriented with respect to the β-lactam ring to be acylated by AZT (AZT C2···Oγ Ser_{64} distance of 3.68 ± 0.44 Å, and AZT C2···Oγ−Cβ Ser_{64} and AZT N1−C2−O9···Oγ Ser_{64} angles of 93 ± 18° and −80 ± 10°, respectively). In this respect, it is interesting to note that the Lys67Arg mutation reinforces the Ser_{64} OγH···$^{-}$Oη Tyr_{150} contact, which is present during only 28% of the TYN150−AZT⁻ trajectory. Other active site contacts are similar along the ARG67−TYN150−AZT⁻ trajectory and in the previously described TYN150−AZT⁻ state.

DISCUSSION

Native Form of the Class C β-Lactamase in Aqueous Solution. In principle, the comparison of the interresidue contacts observed along the MD simulations with those present in the initial X-ray structure could help to identify the most probable configuration of the *C. freundii* β-lactamase. However, no single theoretical model can reproduce all the interresidue contacts observed in the solid-state structure. In terms of their free energies, the LYS and LYN315 configurations are clearly above the LYN67 and TYN150 states by roughly 10−15 kcal/mol. The TYN150 configuration is only ~1 kcal/mol below LYN67. However, if the statistical imprecision of the individual QM-PBSA free energies (6−7 kcal/mol) is taken into account, a clear-cut prediction cannot be made on the basis of the ΔG value, and therefore, either the LYN67 or the TYN150 state could be accessible for the free enzyme in solution.

Although our simulations do not solve by themselves the controversy between the former electrostatic calculations (*30*), which have predicted a low pK_a value for Tyr_{150} of 4−8, and the ^{13}C NMR titration experiments (*29*), which have suggested that the pK_a of Tyr_{150} is well above 11 in the substrate-free form, they clearly indicate that the actual energy difference between the LYN67 and TYN150 configurations should not be large and that a LYN67 ⇄ TYN150 equilibrium might be possible. Nevertheless, it may be interesting to note that the LYN67 state seems more compatible with the ^{13}C NMR titration experiments performed in the wild type and in the Lys67Cys mutant of the *C. freundii* β-lactamase. In the LYN67 state, the Lys67Cys mutation would conserve the global charge in the vicinity of the Tyr_{150} side chain, explaining thus why the Tyr_{150} pK_a value remains virtually unchanged after the mutation.

Binding of AZT to the Class C β-Lactamase Active Site. The dynamical evolution of the β-lactamase−AZT complex was explored by carrying out MD simulations differing in the charge configuration of the Lys_{67}, Tyr_{150}, and Lys_{315} residues and in the protonation state of the AZT inhibitor (anionic or dianionic). The dianionic form of AZT results in β-lactamase−inhibitor complexes that are not favorable for catalysis, as revealed by the structural and energetic analyses. On the other hand, in three of the four simulations with monoanionic AZT, the inhibitor adopts an orientation that is potentially reactive and the nucleophilic serine establishes direct or assisted contacts with the base catalyst (Lys_{67}, Tyr_{150}, or Lys_{315}). However, the free energy calculations point out that the LYN67−AZT⁻ configuration is significantly more stable, by around 20−28 kcal/mol, than the TYN150−AZT⁻ and LYN315−AZT⁻ states. Therefore, we propose that AZT binds to the *C. freundii* active site in its anionic form and that, upon formation of the β-lactamase−AZT noncovalent complex, the neutral form of Lys_{67} becomes clearly stabilized to give the kinetically active configuration.

Implications for the Acylation Mechanism of the C. freundii Enzyme. Consideration of the binding of an antibiotic to the class C β-lactamase active site leads to a firm theoretical prediction about the mechanistic role of the neutral Lys_{67} amino group as the proton acceptor from Ser_{64} during acylation of the *C. freundii* enzyme by aztreonam. This identification of Lys_{67} as the base catalyst for this particular enzyme−ligand association is well grounded in the structural and energetic features exhibited by the LYN67−AZT^- model. We also note that the LYN67−AZT^- model is in agreement with kinetic and mutagenesis experimental results for the AmpC β-lactamase reacting with slowly hydrolyzed substrates such as aztreonam (*62*). In this case, the mutation of Tyr_{150} to Ser results in a slightly more reactive form of the enzyme, which led the authors to note that Tyr_{150} had no obligatory role in catalysis (*62*).

Could the neutral Lys_{67} residue act as the base catalyst for the rest of the class C substrates (cephalosporins, carbapenems, etc.)? On the basis of the nature and the stability of intraprotein and protein−ligand contacts characteristic of the LYN67−AZT^- model, it can be reasonably expected that a neutral Lys_{67} amino group could be stable and play a similar role in the presence of rapidly hydrolyzed substrates. In this respect, it is interesting to note here that the crystal structure of the Ser64Gly mutant of the AmpC β-lactamase in complex with cephalothin shows that the β-lactam carboxylate group accepts a hydrogen bond from the Tyr_{150} side chain (*15*). This interaction is clearly incompatible with the presence of a negatively charged Tyr_{150} residue in the noncovalent complex.

It must be noted that mutagenesis experiments are not conclusive about the protonation state and mechanistic role of the Tyr_{150}/Lys_{67} pair. For example, mutating Tyr_{150} decreases the catalytic efficiency from only 10- to 1000-fold depending on the substrate and mutant being studied (*25*, *62*). The Lys67Gln, Lys67Thr, and Lys67Glu mutants of class C β-lactamases are nearly inactive, in consonance with the proposed catalytic role of Lys_{67}; however, the Lys67Arg mutant exhibits an appreciable activity above pH 7.5, and for some poor substrates of the wild-type enzyme, the k_{cat} values are even increased (*23*, *24*). Why does the Lys67Arg mutant of the *C. freundii* enzyme retain a significant amount of activity? The resolution of this apparent paradox is possible on the basis of the computational observation that the LYN67 and TYN150 configurations of the wild-type *C. freundii* enzyme are very close in energy. Hence, it can be reasonably expected that the Lys67Arg mutation would lead to the corresponding ARG67−TYN150 state characterized by the anionic form of Tyr_{150}. This configuration can be kinetically active as shown by the MD simulation of the Lys67Arg mutant of the *C. freundii* β-lactamase in complex with aztreonam. Thus, the ARG67−TYN150−AZT^- configuration turns out to be characterized by a stable Ser_{64} OγH$\cdots^-$Oη Tyr_{150} contact and a proper orientation of the β-lactam ring in the enzyme active site. Therefore, in the Lys67Arg mutant of the *C. freundii* class C β-lactamase, the anionic Tyr_{150} side chain could act as the base catalyst during acylation.

On the basis of the results obtained by combinatorial scanning mutagenesis that screened more than 1000 variants of the class C P99 enzyme, it has been proposed that catalysis in the class C β-lactamases is affected by a hydrogen bonding network in the active site and that no single residue acts as the catalytic *general* base (*26*). We believe that our simulations add new molecular details to this proposal by discussing the joint ability of the Lys_{67}/Tyr_{150} pair for catalysis. As mentioned above, the Lys_{67} NζH_2/Tyr_{150} OηH and Lys_{67} NζH_3^+/Tyr_{150} Oη^- states in the unbound class C enzyme should be close in terms of free energy. We also found that their relative stability can be modulated by desolvation and protein flexibility effects upon aztreonam binding to give the noncovalent prereactive complex. We expect that binding of other class C substrates and/or formation of the acyl−enzyme species might alter the proton configuration of the Lys_{67}/Tyr_{150} pair. As a matter of fact, quite similar considerations on the Lys_{67}/Tyr_{150} pair have been expressed by Adediran and Pratt in their interpretations of the β-secondary and solvent deuterium kinetic effects on the catalysis exerted by the class C P99 enzyme (*63*). Thus, these authors have suggested that the proton configuration in the noncovalent enzyme−substrate complex may be substrate-dependent and that conversion of the ionic Lys_{67}/Tyr_{150} pair into its neutral form could occur via substrate binding. Taking into account the earlier proposals as well as the theoretical results described above, we suggest that a reversible Lys_{67} NζH_2/Tyr_{150} OηH $\rightleftarrows$ Lys_{67} NζH_3^+/Tyr_{150} Oη^- process could be very catalytically efficient. On one hand, the nucleophilic attack during the acylation step could be triggered by the Ser_{64} OγH $\leftarrow$:NζH_2 Lys_{67} proton transfer, while the Tyr_{150} OηH group could donate a proton to the leaving β-lactam N atom. On the other hand, an anionic Tyr_{150} Oη^- group may activate the hydrolytic water molecule that attacks the acyl−enzyme intermediate during the deacylation process. In principle, the same chemical mechanism could occur in the evolutionarily related PBP proteins such as the DD-peptidase from *Streptomyces* R61 (much in common in the kinetic properties of the two families of enzymes). Moreover, a similar computational study has suggested that the Lys_{38}/Lys_{213} pair of residues in the DD-transpeptidase enzyme from *Streptomyces* K15 could constitute a flexible base catalyst at different mechanistic steps (*50*).

ACKNOWLEDGMENT

We are grateful to the MEC (Spain) for allocation of computer time at the CIEMAT and at the Centro Nacional de Supercomputación (Barcelona Supercomputer Center). D.S. thanks professors D. G. Truhlar and M. Elstner for providing him with copies of the AMSOL and DFT-TB programs, respectively.

SUPPORTING INFORMATION AVAILABLE

Tables S1−S7 and Figures S1−S3, including methods and results of the QM calculations on small cluster models. Two ZIP files containing the AZT parameters in a format suitable for LEaP. Three ZIP files containing selected PM3/AMBER-optimized snapshots in PDB format of the LYN67, TYN150, and LYN67−AZT models. This material is available free of charge via the Internet at http://pubs.acs.org.

REFERENCES

1. Walsh, C. (2000) Molecular mechanisms that confer antibacterial drug resistance, *Nature 406*, 775−781.
2. Wright, G. D. (2000) Resisting resistance: New chemical strategies for battling superbugs, *Chem. Biol. 7*, 127−132.

3. Fisher, J. F., Meroueh, S. O., and Mobashery, S. (2005) Bacterial resistance to β-lactam antibiotics: Compelling opportunism, compelling opportunity, *Chem. Rev. 105*, 395−424.
4. Bush, K., Jacoby, G. A., and Medeiros, A. A. (1995) A functional classification scheme for β-lactamases and its correlation with molecular structure, *Antimicrob. Agents Chemother. 39*, 1211−1233.
5. Maiti, S. N., Philips, O. A., Micetich, R. G., and Livermore, D. M. (1998) β-Lactamase inhibitors: Agents to overcome bacterial resistance, *Curr. Med. Chem. 5*, 441−456.
6. Beceiro, A., and Bou, G. (2004) Class C β-lactamases: An increasing problem worldwide, *Rev. Med. Microbiol. 15*, 141−152.
7. Oefner, C., D'Arcy, A., Daly, J. J., Gubernator, K., Charnas, R. L., Heinze, I., Hubschwerlen, C., and Winkler, F. K. (1990) Refined crystal structure of β-lactamase from *Citrobacter freundii* indicates a mechanism for β-lactam hydrolysis, *Nature 343*, 284−288.
8. Lobkovsky, E., Moews, P. C., Liu, H., Zhao, H., Frere, J. M., and Knox, J. R. (1993) Evolution of an enzyme activity: Crystallographic structure at 2 Å resolution of cephalosporinase from the AmpC gene of *Enterobacter cloacae* P99 and comparison with a class A penicillinase, *Proc. Natl. Acad. Sci. U.S.A. 90*, 11257−11261.
9. Usher, K. C., Blaszczak, L. C., Weston, G. S., Shoichet, B. K., and Remington, S. J. (1998) Three-dimensional structure of AmpC β-lactamase from *Escherichia coli* bound to a transition-state analogue: Possible implications for the oxyanion hypothesis and for inhibitor design, *Biochemistry 37*, 16082−16092.
10. Crichlow, G. V., Kuzin, A. P., Nukaga, M., Mayama, K., Sawai, T., and Knox, J. R. (1999) Structure of the extended-spectrum class C β-lactamase of *Enterobacter cloacae* GC1, a natural mutant with a tandem tripeptide insertion, *Biochemistry 38*, 10256−10261.
11. Patera, A., Blaszczak, L. C., and Shoichet, B. K. (2000) Crystal structures of substrate and inhibitor complexes with AmpC β-lactamase: Possible implications for substrate-assisted catalysis, *J. Am. Chem. Soc. 122*, 10504−10512.
12. Powers, R. A., Caselli, E., Focia, P. J., Prati, F., and Shoichet, B. K. (2001) Structures of ceftazidime and its transition-state analog in complex with AmpC β-lactamase: Implications for resistance mutations and inhibitor design, *Biochemistry 40*, 9207−9214.
13. Trehan, I., Beadle, B. M., and Shoichet, B. K. (2001) Inhibition of AmpC β-lactamase through a destabilizing interaction in the active site, *Biochemistry 40*, 7992−7999.
14. Beadle, B. M., and Shoichet, B. K. (2002) Structural basis for imipenem inhibition of class C β-lactamases, *Antimicrob. Agents Chemother. 46*, 3978−3980.
15. Beadle, B. M., Trehan, I., Focia, P. J., and Shoichet, B. K. (2002) Structural milestones in the reaction pathway of an amide hydrolase: Substrate, acyl, and product complexes of cephalothin with AmpC β-lactamase, *Structure 10*, 413−424.
16. Meroueh, S. O., Minasov, G., Lee, W., Shoichet, B. K., and Mobashery, S. (2003) Structural aspects for evolution of β-lactamases from penicillin-binding proteins, *J. Am. Chem. Soc. 125*, 9612−9618.
17. Nukaga, M., Abe, T., Venkatesan, A. M., Mansour, T. S., Bonomo, R. A., and Knox, J. R. (2003) Inhibition of class A and class C β-lactamases by penems: Crystallographic structures of a novel 1,4-thiazepine intermediate, *Biochemistry 42*, 13152−13159.
18. Roth, T. A., Minasov, G., Morandi, S., Prati, F., and Shoichet, B. K. (2003) Thermodynamic cycle analysis and inhibitor design against β-lactamase, *Biochemistry 42*, 14483−14491.
19. Wouters, J., Fonze, E., Frere, J.-M., and Charlier, P. (2003) Crystal structure of *Enterobacter cloacae* 908R class C β-lactamase bound to iodo-acetamido-phenyl boronic acid, a transition-state analogue, *Cell. Mol. Life Sci. 60*, 1764.
20. Nukaga, M., Kumar, S., Nukaga, K., Pratt, R. F., and Knox, J. R. (2004) Hydrolysis of third-generation cephalosporins by class C β-lactamases. Structures of a transition state analog of cefotaxime in wild-type and extended spectrum enzymes, *J. Biol. Chem. 279*, 9344.
21. Tondi, D., Morandi, F., Bonnet, R., Costi, M. P., and Shoichet, B. K. (2005) Structure-based optimization of a non-β-lactam lead results in inhibitors that do not up-regulate β-lactamase expression in cell culture, *J. Am. Chem. Soc. 127*, 4632−4639.
22. Michaux, C., Charlier, P., Frere, J.-M., and Wouters, J. (2005) Crystal structure of Brl 42715, C6-(N1-methyl-1,2,3-triazolyl-methylene)penem, in complex with *Enterobacter cloacae* 908R β-lactamase: Evidence for a stereoselective mechanism from docking studies, *J. Am. Chem. Soc. 127*, 3262−3263.
23. Tsukamoto, K., Tachibana, K., Yamazaki, N., Ishii, Y., Ujie, K., Nishida, N., and Sawai, T. (1990) Role of lysine-67 in the active site of class C β-lactamase from *Citrobacter freundii* GN346, *Eur. J. Biochem. 188*, 15−22.
24. Monnaie, D., Dubus, A., and Frère, J.-M. (1994) The role of lysine-67 in a class C β-lactamase is mainly electrostatic, *Biochem. J. 304*, 1−4.
25. Dubus, A., Ledent, P., Lamotte-Brasseur, J., and Frère, J.-M. (1996) The roles of residues Tyr150, Glu272, and His314 in class C β-lactamases, *Proteins: Struct., Funct., Genet. 25*, 473−485.
26. Goldberg, S. D., Iannuccilli, W., Nguyen, T., Ju, J., and Cornish, V. W. (2003) Identification of residues critical for catalysis in a class C β-lactamase by combinatorial scanning mutagenesis, *Protein Sci. 12*, 1633−1645.
27. Monnaie, D., Dubus, A., Cooke, D., Marchand-Brynaert, J., Normark, S., and Frère, J.-M. (1994) Role of residue Lys315 in the mechanism of action of the *Enterobacter cloacae* 908R β-lactamase, *Biochemistry 33*, 5193−5201.
28. Zhang, Z., Yu, Y., Musser, J. M., and Palzkill, T. (2001) Amino acid sequence determinants of extended spectrum cephalosporin hydrolysis by the class C P99 β-lactamase, *J. Biol. Chem. 276*, 46568−46574.
29. Kato-Toma, Y., Iwashita, T., Masuda, K., Oyama, Y., and Ishiguro, M. (2003) pK_a measurements from nuclear magnetic resonance of tyrosine-150 in class C β-lactamase, *Biochem. J. 371*, 175−181.
30. Lamotte-Brasseur, J., Dubus, A., and Wade, R. C. (2000) pK_a calculations for class C β-lactamases: The role of Tyr150, *Proteins: Struct., Funct., Genet. 40*, 23−28.
31. Bulychev, A., Massova, I., Miyashita, K., and Mobashery, S. (1997) Nuances of mechanisms and their implications for evolution of the versatile β-lactamase activity: From biosynthetic enzymes to drug resistance factors, *J. Am. Chem. Soc. 119*, 7619−7625.
32. Fenollar-Ferrer, C., Donoso, J., Frau, J., and Muñoz, F. (2005) Molecular modeling of the Henry-Michaelis and acyl-enzyme complexes between imipenem and *Enterobacter cloacae* P99 β-lactamase, *Chem. Biodiversity 2*, 645−656.
33. Gherman, B. F., Goldberg, S. D., Cornish, V. W., and Friesner, R. A. (2004) Mixed quantum mechanical/molecular mechanical (QM/MM) study of the deacylation reaction in a penicillin binding protein (PBP) versus in a class C β-lactamase, *J. Am. Chem. Soc. 126*, 7652−7664.
34. Fenollar-Ferrer, C., Frau, J., Donoso, J., and Muñoz, F. (2003) The role of β-lactam carboxyl group on binding of penicillins and cephalosporins to class C β-lactamases, *Proteins: Struct., Funct., Genet. 51*, 442−452.
35. Wilkinson, A.-S., Bryant, P. K., Meroueh, S. O., Page, M. G. P., Mobashery, S., and Wharton, C. W. (2003) A dynamic structure for the acyl-enzyme species of the antibiotic aztreonam with the *Citrobacter freundii* β-lactamase revealed by infrared spectroscopy and molecular dynamics simulations, *Biochemistry 42*, 1950−1957.
36. Sykes, R. B., Bonner, D. P., Bush, K., and Georgopapadakou, N. H. (1982) Aztreonam (SQ 26,776), a synthetic monobactam specifically active against aerobic gram-negative bacteria, *Antimicrob. Agents Chemother. 21*, 85−92.
37. Jorgensen, W. L., Chandrasekhar, J., Madura, J., Impey, R. W., and Klein, M. L. (1983) Comparison of simple potential functions for the simulation of liquid water, *J. Chem. Phys. 79*, 926−935.
38. Schafmeister, C., Ross, W. S., and Romanovski, V. (1995) *LEaP*, University of California, San Francisco.
39. Cornell, W. D., Cieplak, P., Bayly, C. I., Gould, I. R., Merz, K. M., Jr., Ferguson, D. M., Spellmeyer, D. C., Fox, T., Caldwell, J. W., and Kollman, P. A. (1995) A second generation force field for the simulation of proteins, nucleic acids, and organic molecules, *J. Am. Chem. Soc. 117*, 5179−5197.
40. Case, D. A., Darden, T. A., Cheatham, T. E. I., Simmerling, C. L., Wang, J., Duke, R. E., Luo, R., Merz, K. M., Wang, B., Pearlman, D. A., Crowley, M., Brozell, S., Tsui, V., Gohlke, H., Mongan, J., Hornak, V., Cui, G., Beroza, P., Schafmeister, C., Caldwell, J. W., Ross, W. S., and Kollman, P. A. (2004), *AMBER 8*, University of California, San Francisco.
41. Berendsen, H. J. C., Potsma, J. P. M., van Gunsteren, W. F., DiNola, A. D., and Haak, J. R. (1984) Molecular dynamics with coupling to and external bath, *J. Chem. Phys. 81*, 3684−3690.

42. Essman, V., Perera, L., Berkowitz, M. L., Darden, T., Lee, H., and Pedersen, L. G. (1995) A smooth Particle-Mesh-Ewald method, *J. Chem. Phys. 103*, 8577−8593.
43. Kraulis, P. J. (1991) Molscript: A program to produce both detailed and schematic plots of protein structures, *J. Appl. Crystallogr. 24*, 946−950.
44. Merritt, E. A., and Bacon, D. J. (1997) Raster3D: Photorealistic molecular graphics., *Methods Enzymol. 277*, 505−524.
45. Florey, K. (1988) Aztreonam, in *Analytical profiles of drug substances*, pp 1−39, Academic Press, New York.
46. Sowek, J. A., Singer, S. B., Ohringer, S., Malley, M. F., Dougherty, T. J., Gougoutas, J. Z., and Bush, K. (1991) Substitution of lysine at position 104 or 240 of Tem-1_{ptz18r} β-lactamase enhances the effect of serine-164 substitution on hydrolysis or affinity for cephalosporins and the monobactam aztreonam, *Biochemistry 30*, 3179−3188.
47. Frisch, M. J., Trucks, G. W., Schlegel, H. B., Scuseria, G. E., Robb, M. A., Cheeseman, J. R., Zakrzewski, V. G., Montgomery, J. A., Stratmann, R. E., Jr., Burant, J. C., Dapprich, S., Millam, J. M., Daniels, A. D., Kudin, K. N., Strain, M. C., Farkas, O., Tomasi, J., Barone, V., Cossi, M., Cammi, R., Mennucci, B., Pomelli, C., Adamo, C., Clifford, S., Ochterski, J., Petersson, G. A., Ayala, P. Y., Cui, Q., Morokuma, K., Malick, D. K., Rabuck, A. D., Raghavachari, K., Foresman, J. B., Cioslowski, J., Ortiz, J. V., Stefanov, B. B., Liu, G., Liashenko, A., Piskorz, P., Komaromi, I., Gomperts, R., Martin, R. L., Fox, D. J., Keith, T., Al-Laham, M. A., Peng, C. Y., Nanayakkara, A., Gonzalez, C., Challacombe, M., Gill, P. M. W., Johnson, B., Chen, W., Wong, M. W., Andres, J. L., Gonzalez, C., Head-Gordon, M., Replogle, E. S., and Pople, J. A. (1998) *Gaussian98*, Gaussian, Inc., Pittsburgh, PA.
48. Kollman, P. A., Massova, I., Reyes, C., Kuhn, B., Huo, S., Chong, L., Lee, M., Lee, T., Duan, Y., Wang, W., Donini, O., Cieplak, P., Srinivasan, J., Case, D. A., and Cheatham, T. E. (2000) Calculating structures and free energies of complex molecules: Combining molecular mechanics and continuum models, *Acc. Chem. Res. 33*, 889−897.
49. Gohlke, H., and Case, D. A. (2003) Converging free energy estimates: MM-PB(GB)SA studies on the protein−protein complex Ras−Raf, *J. Comput. Chem. 25*, 238−250.
50. Díaz, N., Sordo, T. L., and Suárez, D. (2005) Insights into the base catalysis exerted by the DD-transpeptidase from *Streptomyces K15*: A molecular dynamics study, *Biochemistry 44*, 3225−3240.
51. Yang, W., and Lee, T.-S. (1995) A density-matrix form of the divide-and-conquer approach for electronic structure calculations of large molecules, *J. Chem. Phys. 103*, 5674−5678.
52. Dixon, S. L., and Merz, K. M., Jr. (1997) Fast, accurate semiempirical molecular orbital calculations for macromolecules, *J. Chem. Phys. 107*, 879−893.
53. Wang, B., Raha, K., Liao, N., Peters, M. B., Kim, H., Westerhoff, L. M., Wollacott, A. M., van der Vaart, A., Gogonea, V., Suarez, D., Dixon, S. L., Vincent, J. J., Brothers, E. N., and Merz, K. M. J. (2005) *DIVCON 4.0*, QuantumBio Inc., State College, PA.
54. Stewart, J. J. P. (1989) Optimization of parameters for semiempirical methods I. Method, *J. Comput. Chem. 10*, 209−220.
55. Gogonea, V., and Merz, K. M., Jr. (1999) Fully quantum mechanical description of proteins in solution. Combining linear scaling quantum mechanical methodologies with the Poisson−Boltzmann equation, *J. Phys. Chem. A 103*, 5171−5178.
56. Orozco, M., and Luque, F. J. (2000) Theoretical methods for the description of the solvent effect in biomolecular systems, *Chem. Rev. 100*, 4187−4225.
57. Elstner, M., Hobza, P., Frauenheim, T., Suhai, S., and Kaxiras, E. (2001) Hydrogen bonding and stacking interactions of nucleic acid base pairs: A density-functional-theory based treatment, *J. Chem. Phys. 114*, 5149−5154.
58. Elstner, M., Porezag, D., Jungnickel, G., Elsner, J., Haugk, M., Frauenheim, T., Suhai, S., and Seifert, G. (1998) Self-consistent-charge density-functional tight-binding method for simulations of complex materials properties, *Phys. Rev. B 58*, 7260−7268.
59. Miller, K. J. (1990) Additivity methods in molecular polarizability, *J. Am. Chem. Soc. 112*, 8533−8542.
60. Halgren, T. A. (1992) Representation of van der Waals (vdw) interactions in molecular mechanics force fields: Potential form, combination rules, and vdw parameters, *J. Am. Chem. Soc. 114*, 7827−7843.
61. Vondrásek, J., Bendová, L., Klusák, V., and Hobza, P. (2005) Unexpectedly strong energy stabilization inside the hydrophobic core of small protein rubredoxin mediated by aromatic residues: Correlated ab initio quantum chemical calculations, *J. Am. Chem. Soc. 127*, 2615−2619.
62. Dubus, A., Normark, S., Kania, M., and Page, M. G. P. (1994) The role of tyrosine 150 in catalysis of β-lactam hydrolysis by AmpC β-lactamase from *Escherichia coli* investigated by site-directed mutagenesis, *Biochemistry 33*, 8577−8586.
63. Adediran, S. A., and Pratt, R. F. (1999) β-Secondary and solvent deuterium kinetic isotope effects on catalysis by the *Streptomyces* R61 DD-peptidadse: Comparison with a structurally similar class C β-lactamase, *Biochemistry 38*, 1469−1477.

BI051600J